

deepMiRGene: Deep Neural Network based Precursor microRNA Prediction

Seunghyun Park, Seonwoo Min, Hyun-soo Choi, and Sungroh Yoon*

SRYOON@SNU.AC.KR

Department of Electrical and Computer Engineering, Seoul National University, Seoul 151-744, Korea

Abstract

Since microRNAs (miRNAs) play a crucial role in post-transcriptional gene regulation, miRNA identification is one of the most essential problems in computational biology. miRNAs are usually short in length ranging between 20 and 23 base pairs. It is thus often difficult to distinguish miRNA-encoding sequences from other non-coding RNAs and pseudo miRNAs that have a similar length, and most previous studies have recommended using precursor miRNAs instead of mature miRNAs for robust detection. A great number of conventional machine-learning-based classification methods have been proposed, but they often have the serious disadvantage of requiring manual feature engineering, and their performance is limited as well. In this paper, we propose a novel miRNA precursor prediction algorithm, deepMiRGene, based on recurrent neural networks, specifically long short-term memory networks. deepMiRGene automatically learns suitable features from the data themselves without manual feature engineering and constructs a model that can successfully reflect structural characteristics of precursor miRNAs. For the performance evaluation of our approach, we have employed several widely used evaluation metrics on three recent benchmark datasets and verified that deepMiRGene delivered comparable performance among the current state-of-the-art tools.

1. Introduction

A miRNA (microRNA) is a small non-coding RNA that plays a crucial role in post-transcriptional gene regulation by attaching itself to the 3' untranslated region of the target mRNA (Lee et al., 1993). There are a number of research problems related to miRNA, including the search

for miRNA itself or the miRNA regulation target, messenger RNA (mRNA). Among the many problems, how to computationally identify miRNAs has been one of the most significant problems. From the engineering point of view, miRNA identification can be understood as a binary classification problem that classifies input sequences into miRNA or non-miRNA. miRNA follows the sequence of primary miRNA into precursor mRNA (pre-miRNA), then into mature miRNA and RNA-induced silencing complex (Bartel, 2004). Mature miRNAs are usually short, having 20 to 23 base pairs (bp), and thus it is difficult to identify them using only sequence patterns. In order to identify miRNAs, most computational approaches thus focus on detecting pre-miRNAs since they are usually longer (approximately 80bp) and also have the distinguishing feature of a stem-loop secondary structure. The advent of next generation sequencing has made it possible to detect RNAs even in low concentrations. However, it has also led to the discovery of many other novel RNAs besides miRNA, such as siRNA, piRNA, and degradation products of ribosomal RNA and transfer RNA, leading to an increase in identification subjects and consequently raising the problem of high false positives (Kang & Friedländer, 2015).

Many computational approaches to identifying miRNA have been proposed and can be divided into two categories: conservation and rule-based methodologies and machine-learning-based methodologies (Kleftogiannis et al., 2013). Since a sufficient number of miRNAs for machine learning are now available, currently utilized tools are mostly machine-learning-based. Specific machine learning algorithms used are diverse. MiPred (Jiang et al., 2007), microPred (Batuwita & Palade, 2009), triplet-SVM (Xue et al., 2005), and miRBoost (Tempel et al., 2015) uses the support vector machine (SVM); CSHMM (Agarwal et al., 2010) has adopted the hidden Markov model (HMM) and additionally utilized context-sensitive characteristics to consider secondary structures more carefully; and MIRENA (Mathelier & Carbone, 2010) uses five rule-based schemes.

What the mentioned approaches have in common is that they use hand-crafted features that include structural and folding energy information of miRNA precursors. For ex-

ample, the frequency of triplets appearing in the loop, the stem length, and minimum free energy are widely used features. Some studies have even argued that the performance of machine learning-based tools is more dependent on input feature sets rather than the specific machine-learning algorithms (de ON Lopes et al., 2014). Therefore, most previous approaches have focused on either searching for novel features or combining the existing features using ensemble algorithms. Indeed, high accuracy was reported for miRBoost and microPred using more than 100 known features. Nonetheless, most of the existing tools still suffer from the low-sensitivity issue.

In this paper, we propose deepMiRGene, which uses recurrent neural networks (RNNs), specifically long short-term memory (LSTM) networks, to learn sequence patterns and folding structure. **The most important contribution of the proposed approach is that it does not require any painful manual feature engineering.** This method takes advantage of end-to-end deep learning, which only requires simple preprocessing instead of a considerable amount of domain knowledge to design hand-crafted features. Since miRNA has a palindromic secondary structure, it is difficult to immediately apply an LSTM network. To solve such difficulties, **we propose a novel method for learning the palindromic secondary structure of precursor miRNA.** Furthermore, **deepMiRGene delivers superior performance, outperforming all compared alternatives in terms of sensitivity and specificity on the benchmarking datasets.** deepMiRGene also gives the best performance in cross-species data, even though many differences exist between the features among the different species. Our approach shows the possibility of rediscovering intrinsic features in a data-driven fashion and is expected to bring novel biological knowledge as an automated and effective feature extractor.

2. Related Work

2.1. RNN and LSTM

RNN is a deep learning structure designed to learn variable length sequential data. Figure 1(A) shows the basic structure of RNN. The core aspect of RNN is that unlike other structures, RNN processes input data one element at a time and stores past information implicitly using cyclic connections of hidden units (LeCun et al., 2015). Since time-unfolded RNN is an even deeper structure than DNN or CNN, it is difficult to learn long-term dependency with simple perceptron hidden units due to the gradient vanishing problem (Bengio et al., 1994). Therefore most RNN research uses more sophisticated hidden units that operate as some kind of memory cell. LSTM (Hochreiter & Schmidhuber, 1997), shown in Figure 1(B), is the most well-known example. Besides cyclic connections storing the state vec-

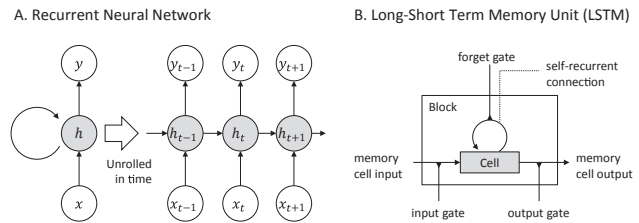


Figure 1. (A) Basic structure of recurrent neural network (LeCun et al., 2015) and (B) diagram of LSTM cell unit (deeplearning.net).

tor, LSTM uses multiplicative gates to learn when to input, output, and forget to produce better performance with RNN.

2.2. Palindromic Structure of Folded miRNA Precursor

Precursor miRNA exists in the form of a base-paired double helix rather than a single strand, and its structural information is important in its identification. RNAfold (Hofacker, 2003) is a widely used tool to predict the secondary structure from a sequence. It predicts the thermodynamically stable secondary structure of a given RNA sequence by calculating the minimum free energy (MFE) and the base-pairing probabilities (Lorenz et al., 2011). The ordinary secondary structure of a precursor miRNA is shown in Figure 2 (A). In dot-bracket notation (DBN), one of the widely used expression methods for secondary structure, unpaired nucleotides are represented as $.$ and paired nucleotides are represented as opening “(”s and closing “)”s. This structure consisting of helices and a loop, is called stem-loop or hairpin structure. On the other hand, pseudo miRNA precursors and other noncoding RNAs have a structure that distinguishes them from true precursor miRNAs, such as asymmetric bulges and multiple loops. Although some false positives exist due to limitations of prediction algorithms and unpredictable structures, like pseudoknots (Lyngsø, 2004), secondary structure is still one of the most essential features for identifying precursor miRNAs.

A notable characteristic of the stem-loop structure of a precursor miRNA is that it is palindromic. As shown in Figure 2(B), the left side of the stem, which is a forward strand ($5' \rightarrow 3'$), and the right side of the stem, which is a backward strand ($3' \rightarrow 5'$), make complementary matches, forming a helix. Therefore, from the backward strand point of view, the stem-loop structure of the precursor miRNA constitutes a form of stack. However, since general LSTM networks are designed to learn sequential data and constitute a form of queue, it requires special preprocessing,

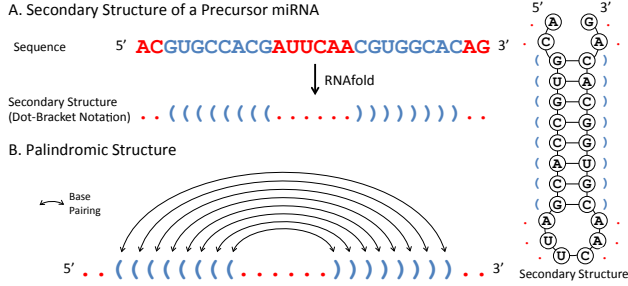


Figure 2. The secondary structure of a precursor miRNA and its palindromic structure. (A) The left means the sequence of a precursor miRNA and the right represents the secondary structure of a given sequence. Dot-bracket notation (DBN), below the sequence, is the method for describing a secondary structure. Unpaired nucleotides are represented as “.” and base-paired nucleotides are represented as opening “(”s and closing “)”s. (B) A Palindrome in secondary structure. The forward strand (5' → 3') on the left side of the middle point and the backward strand (3' → 5') on the right side of the middle point match complementarily.

as reversing a structure, which is discussed further in Section 3.

3. Methodology

An overview of the proposed method is shown in Figure 3, and Algorithm 1 presents more details of the proposed approach. In the preprocessing step, the secondary structure of the input miRNA sequence is generated and split into a forward structure and a backward structure. Then in the neural network layers, RNN model parameters are trained according to the input data. The miRNA sequence, the forward structure, and the reversed backward structure are entered into the embedding layer. Finally, through three LSTM layers and fully connected layers, prediction results are produced.

3.1. Preprocessing

The secondary structure is generated using RNAfold and can be divided into forward structure, which has a direction of 5' to 3', and backward structure, which has a direction of 3' to 5'. In this study, based on the loop center of the secondary structure, the 5' side is categorized as forward and the 3' side is categorized as backward. If multiple loops exist, the middle point between the start point of the 5' closest loop and the end point of the 5' farthest loop is used as the basis.

3.2. Construction of RNN Model

Embedding Layers: miRNA sequence and structure are categorical data that have observable states of four (A, C, G, U) and three (“(”, “.”, “)”), respectively. Thus word em-

Table 1. The number of datasets used in this study

Type	Human	Cross-species	New pre-miRNAs
Positive set	863	1677	690
Negative set	7422	8266	8246

bedding layers are added to embed the miRNA sequence into four dimension (E_{seq}) and structure into three dimension (E_{f-str} and E_{b-str}). The embedding layer does not use one-hot encoding, but rather adopts weight matrices to learn the proper encoding from data as well.

LSTM Layers: Embedded data streams are entered into three independent LSTM layers. All of the L_{seq} , L_{f-str} , and L_{b-str} layers have 10 hidden nodes as outputs and use hyperbolic tangent and hard sigmoid as their inner activation functions.

Fully Connected Layers: Outputs of three LSTM layers are first connected to two fully connected layers. F_{seq} receives 10-dimension input from L_{seq} , and F_{str} receives 20-dimension input from concatenation of L_{f-str} and L_{b-str} . Both F_{seq} and F_{str} have an output of two dimensions and their concatenation is connected to the final fully connected layer F_{multi} , which has output of two dimensions as well. All fully connected layers use sigmoid function as their activation functions. For regularization, several methods can be used such as dropout or batch normalization (Ioffe & Szegedy, 2015). In this study, we selected dropout with a rate of 0.2.

Training settings are the same as follows. The mean squared error (MSE) is used as an objective function, and Adam (Kingma & Ba, 2014) is used as the optimizer. Adam is one of the gradient descent algorithms, which computes adaptive learning rates for each parameter similar to momentum. In other words, Adam considers the moments of the gradient, such as RMSProp.

3.3. Experimental Setup

Three kinds of benchmark datasets from miRBoost (Tempel et al., 2015) were used. The number of human, cross-species, and new pre-miRNAs datasets is shown in Table 1.

The algorithm is implemented by the Theano (Bastien et al., 2012; Bergstra et al., 2010) and Keras (Chollet, 2015) library. The five fold cross-validations are carried out for all data, and the mini-batch size and training epoch are set as 128 and 500 times, respectively. The experiment was performed on a server consisting of an Intel Xeon E5-2650 and Nvidia Geforce Titan GPU.

Algorithm 1 Precursor miRNA prediction

1: **Input:** $x_s = \langle x_{s,1}, x_{s,2}, \dots, x_{s,|x_s|} \rangle$ where $x_s \in X_s$,
 y
 $\triangleright X$: A set of sequences. $|X_s| = N$
 $\triangleright x_s$: A precursor miRNA sequence with its length of $|x_s|$ and $x_{s,i} \in \{A, C, G, U\}$ for $i = 1, 2, \dots, |x_s|$
 $\triangleright y$: A true label for x_s . $y \in \{0, 1\}$
2: **Param:** m : mini-batch size
3: **Output:** $W = \{w_e, w_l, w_f\}$
 $\triangleright W$: Whole model weights composed of weights of embedding layers (w_e), LSTM layers (w_l), fully connected layers (w_f)
Step 1: Preprocessing (Section 3.1)
4: **for** each sequence in X_s
5: $x_t \leftarrow \text{fold}(x_s)$
 $\triangleright \text{fold}$: A function to predict a secondary structure of a given sequence x_s
 $\triangleright x_t$: A dot-bracket notated secondary structure of given input sequence x_s . $|x_t| = |x_s|$ and $x_t = \langle x_{t,1}, x_{t,2}, \dots, x_{t,|x_t|} \rangle$ where $x_{t,i} \in \{(\cdot, \cdot)\}$ for $i = 1, 2, \dots, |x_t|$
6: $(x_f, x_b) \leftarrow \text{split}(x_t)$
 $\triangleright \text{split}$: A function to split a given secondary structure x_s into a forward structure x_f and a backward structure x_b
 $\triangleright x_f = \langle x_{t,1}, x_{t,2}, \dots, x_{t,k-1} \rangle$ and $x_b = \langle x_{t,k}, x_{t,k+1}, \dots, x_{t,|x_t|} \rangle$ for pre-determined position k
7: $x_r \leftarrow \text{flip}(x_b)$
 $\triangleright \text{flip}$: A function to flip a given structure x_b
 $\triangleright x_r$: The flipped structure of x_b . $x_r = \langle x_{t,|x_t|}, x_{t,|x_t|-1}, \dots, x_{t,k} \rangle$
The outputs of preprocessing are grouped into X_f and X_r where $x_f \in X_f$ and $x_r \in X_r$ respectively
Step 2: Training on neural network (Section 3.2)
8: initializing weights W
9: **for** each epoch
10: **for** m training data of x_s , x_f and x_r randomly picked from dataset X_s, X_f , and X_r

Embedding Layers

11: $x'_s \leftarrow \text{embed}_{\text{seq}}(x_s)$
12: $x'_f \leftarrow \text{embed}_{\text{f-str}}(x_f)$
13: $x'_r \leftarrow \text{embed}_{\text{b-str}}(x_r)$
 $\triangleright \text{embed}$: Embedding layer to return a matrix for an input tuple
 $\triangleright x'_s$ is $|x_s| \times 4$ matrix. x'_f and x'_r are the matrices of $|x_f| \times 3$ and $|x_r| \times 3$, respectively

LSTM Layers

14: $h_s \leftarrow \text{LSTM}_{\text{seq}}(x'_s)$
15: $h_f \leftarrow \text{LSTM}_{\text{f-str}}(x'_f)$
16: $h_r \leftarrow \text{LSTM}_{\text{b-str}}(x'_r)$
 $\triangleright \text{LSTM}$: LSTM layer to return a vector for an input matrix
 $\triangleright h_s, h_f$, and h_r are 10-dim vectors for the output of each LSTM layer.

Fully Connected Layers

17: $y_s \leftarrow \text{fcl}_{\text{seq}}(h_s)$
18: $y_t \leftarrow \text{fcl}_{\text{str}}(h_f \frown h_r)$
 $\triangleright \text{fcl}$: Fully connected layer to return an output vector
 $\triangleright \text{fcl}_{\text{seq}}$: 10-dim input and 2-dim output
 $\triangleright \text{fcl}_{\text{str}}$: 20-dim input and 2-dim output
 $\triangleright \frown$: vector concatenate operation
19: $\hat{y} \leftarrow \text{fcl}_{\text{multi}}(y_s \frown y_t)$
 $\triangleright \text{fcl}_{\text{multi}}$: 4-dim input and 2-dim output

Weights Updating

20: $E \leftarrow -\frac{1}{m} \sum_m (\hat{y} - y)^2$
 $\triangleright E$: Mini-batch training error using mean squared error
21: $W \leftarrow W - \Delta W$
 \triangleright Calculating ΔW based on E using gradient descent optimization algorithm “Adam”

Table 2. Performance evaluation.

	Human				Cross-species				New pre-miRNAs			
Software	<i>SE</i>	<i>SP</i>	F-score	g-mean	<i>SE</i>	<i>SP</i>	F-score	g-mean	<i>SE</i>	<i>SP</i>	F-score	g-mean
<i>miRBoost</i>	0.82	0.98	0.89	0.90	0.84	0.97	0.90	0.90	0.88	0.91	0.89	0.89
<i>CSHMM</i>	0.49	0.99	0.65	0.70	0.42	0.97	0.58	0.64	0.24	0.95	0.37	0.48
<i>triplet-SVM</i>	0.67	0.98	0.79	0.81	0.74	0.96	0.83	0.84	0.41	0.95	0.56	0.62
<i>microPred</i>	0.76	0.99	0.86	0.87	0.82	0.98	0.89	0.90	0.72	0.97	0.82	0.84
<i>MIReNA</i>	0.83	0.92	0.87	0.87	0.80	0.93	0.86	0.86	0.46	0.91	0.59	0.65
<i>deepMiRGene</i>	0.89	0.99	0.93	0.94	0.91	0.98	0.94	0.94	0.88	0.99	0.93	0.94

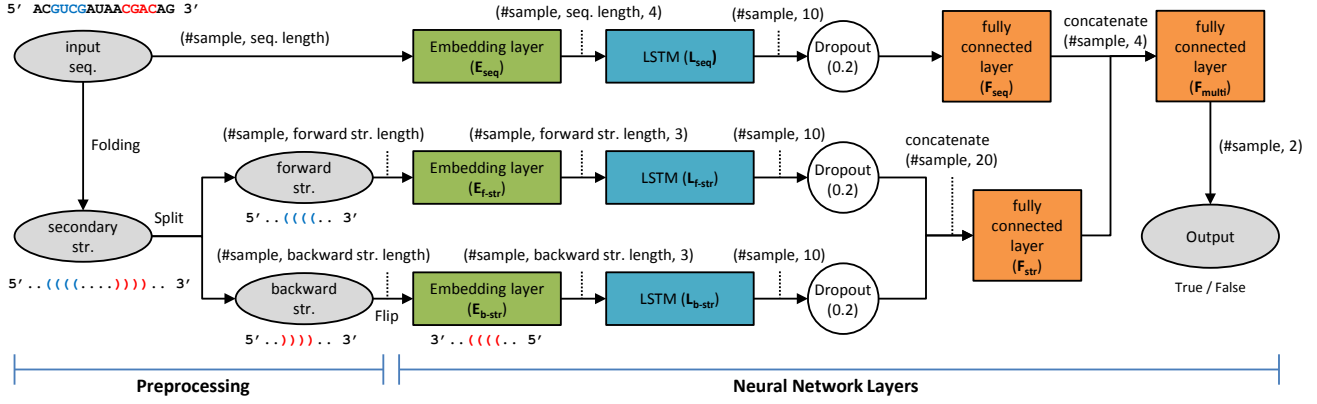


Figure 3. Overview of the proposed method.

4. Experimental Results

4.1. Performance Evaluation

Table 2 shows benchmarking results on three different datasets. Sensitivity and specificity values of all compared tools are based on experimental results of MiRBoost. Evaluation metrics, such as accuracy, positive predictive value (PPV), F-score, Matthews correlation coefficient (MCC), and the geometric mean (g-mean), are dependent on the proportion of positive and negative data in the test dataset. In this paper, we set the proportion equally and calculated the evaluation metrics.

The results show that deepMiRGene gives the best performance in every evaluation metric. In the human dataset, all of the tools maintained high specificity, but deepMiRGene achieved 6 percentage points higher sensitivity than MIRENA and 4 percentage points higher F-score than miRBoost, which are the highest among the conventional tools, respectively. Similarly in the cross-species dataset, the proposed method achieved 7 percentage points higher sensitivity and 4 percentage points higher F-score than miRBoost, which ranks the highest among the conventional tools. Finally in the new pre-miRNAs dataset, although deepMiRGene shows the same level of sensitivity as miRBoost, it achieved the higher specificity by 8 percentage points.

The performance evaluation metrics of deepMiRGene are calculated as follows. A five fold cross-validation was carried out and assuming epoch 450 to 500 as the interval of convergence, we averaged the metric values in the range. Figure 4 shows the change in training loss and evaluation metrics relative to the training epoch number, and the interval of convergence is marked in red in each graph. Parts without values indicate not a number (NaN). Specificity constantly showing a value close to 1 and other metrics showing the increase as the training epoch progresses can

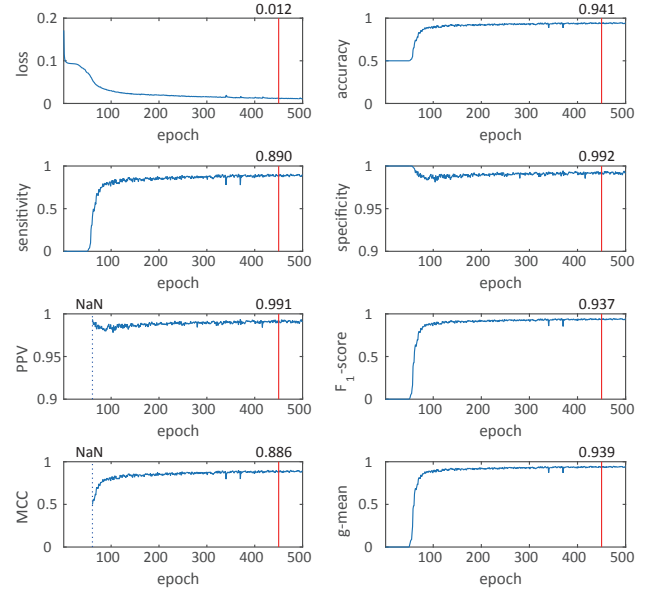


Figure 4. Training loss and seven evaluation metrics using test dataset with a varying epoch.

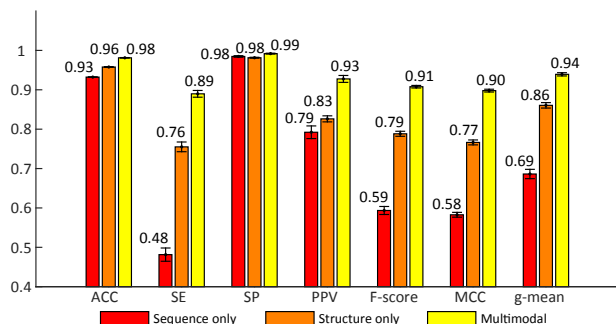


Figure 5. Performance evaluation of the human dataset in cases of using only sequence, only structure, and both sequence and structure (multimodal). Average scores of the 5 fold results are reported together with the error bars.

be understood in terms of imbalance of training data. As in Table 1, negative data are relatively larger than positive data in the training dataset. Therefore, in the early training phase, prediction is biased toward the negative dataset and as learning progresses sufficiently, the prediction is tuned and converged.

4.2. Effect of Multimodality

In this study, we took advantage of both biological sequence information and derived secondary structure information in miRNA classification. To verify the effect of multimodality, we tested cases of either biological sequence or secondary structure information is utilized for the human dataset. As shown in Figure 5, all of the performance metrics are higher when both types of information are used. To be specific, multimodality achieved 41 and 13 percentage points higher sensitivity than when only sequence or structure was utilized, respectively. Similarly, in terms of F-score, multimodality showed 12 and 32 percentage points higher scores. Between sequence and structure information, derived structure information seems to have a more direct effect on accuracy than sequence information.

4.3. Learning Capability of Palindromic Structure

In the proposed method, structure preprocessing of split and flip was used to properly learn palindromic structures. Figure 6 shows the performance comparison in the case of considering the palindromic structure or not. In all of the compared evaluation metrics, considering the palindromic structure produced the better results. Especially, the difference of specificity is up to 22 percentage points. As mentioned in Section 2.2, it is because the general LSTM structure is designed to learn from sequential data. Therefore, we were able to verify that the preprocessing step adopted in the proposed method can help effectively learn palindromic structures.

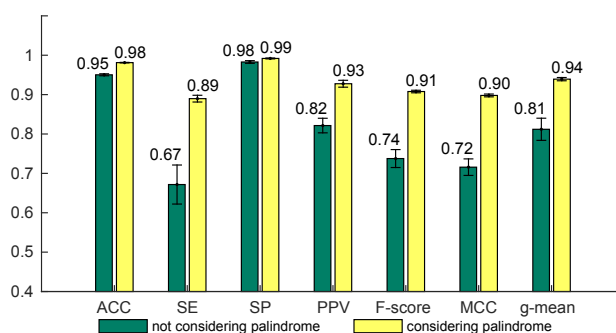


Figure 6. Performance evaluation of human dataset in the cases of considering palindromic structure or not. Average scores of the 5 fold results are reported together with the error bars.

4.4. Visualization of Cell State Transition

RNNs, specifically LSTM network classification methods usually contain features implicitly in the intermediate layer. There is a downside to these high-level features, in that it is difficult to intuitively understand them. Therefore much research is being conducted to find low-level features (Karpathy et al., 2015; Li et al., 2015). Visualization of low-level features is dependent on the problem to be solved; thus a range of high to low level approaches are needed. Many features used in machine-learning-based methodologies, such as microPred and miRBoost, are related to the secondary structure of the precursor miRNA. For example, there is frequency of triplets in the sequence, length of stem and loop structures, folding energy, and so on.

Figure 7 shows the transition of cell states while positive and negative data are being processed by the trained model. LSTM networks in this paper consist of 10 hidden nodes, so for each sequence and structure they are presented as a heatMap. The top parts of (A) and (B) show the cell states related to the sequence, and the bottom shows the cell states related to the structure. In the top red boxes, intensity differences exist between nucleotides (A,U) and (G,C). Since nucleotide pairs of A-U and G-C make hydrogen bonds that have a great influence on the structure of miRNA sequences, differences in the LSTM cell states can be understood as one of the successfully learned structural features. In the bottom red boxes of Figure 7A, most boundaries between the continuous dots (loop/bulge) and the continuous brackets (stem) are clearly distinguishable by the LSTM cell states. However, in the bottom red boxes of Figure 7B, the left side of the backward strand shows different patterns. This is because the corresponding part belongs to the additional loop that deforms the palindromic structure, so it can also be understood as another learned feature to identify negative data. The notable aspect is that hidden nodes with almost no change are observed in both

to-end learning approach that can identify precursor miRNAs using the RNNs, specifically LSTM networks. The proposed method has a major advantage over existing alternatives in that no hand-crafted feature set is needed and it delivers better performance in terms of all the evaluation metrics considered. The structure of a precursor miRNA is a palindromic, which is difficult to learn even with ordinary LSTM or bidirectional LSTM networks. To address this issue, deepMiRGene uses a novel learning scheme in which the secondary structure of the input sequence is divided into the forward and backward streams and each structure stream is learned in a different sequential direction. By applying the proposed learning method, we expect an effective learning process on the data that may have conflicts in temporal direction. In addition, we confirmed the possibility of rediscovering existing structural features by visually inspecting the transition of the LSTM cell states on each position in the sequence.

References

- Agarwal, Sumeet, Vaz, Candida, Bhattacharya, Alok, and Srinivasan, Ashwin. Prediction of novel precursor mirnas using a context-sensitive hidden markov model (cshmm). *BMC bioinformatics*, 11(Suppl 1):S29, 2010.
- Bartel, David P. Micrnas: genomics, biogenesis, mechanism, and function. *cell*, 116(2):281–297, 2004.
- Bastien, Frédéric, Lamblin, Pascal, Pascanu, Razvan, Bergstra, James, Goodfellow, Ian J., Bergeron, Arnaud, Bouchard, Nicolas, and Bengio, Yoshua. Theano: new features and speed improvements. Deep Learning and Unsupervised Feature Learning NIPS 2012 Workshop, 2012.
- Batuwita, Rukshan and Palade, Vasile. micropred: effective classification of pre-mirnas for human mirna gene prediction. *Bioinformatics*, 25(8):989–995, 2009.
- Bengio, Yoshua, Simard, Patrice, and Frasconi, Paolo. Learning long-term dependencies with gradient descent is difficult. *Neural Networks, IEEE Transactions on*, 5(2):157–166, 1994.
- Bergstra, James, Breuleux, Olivier, Bastien, Frédéric, Lamblin, Pascal, Pascanu, Razvan, Desjardins, Guillaume, Turian, Joseph, Warde-Farley, David, and Bengio, Yoshua. Theano: a CPU and GPU math expression compiler. In *Proceedings of the Python for Scientific Computing Conference (SciPy)*, June 2010. Oral Presentation.
- Chollet, François. Keras: Theano-based deep learning library. Code: <https://github.com/fchollet/Documentation>: <http://keras.io>, 2015.
- de ON Lopes, Ivani, Schliep, Alexander, and de Carvalho, André CP de LF. The discriminant power of rna features for pre-mirna recognition. *BMC bioinformatics*, 15(1):1, 2014.
- Hochreiter, Sepp and Schmidhuber, Jürgen. Long short-term memory. *Neural computation*, 9(8):1735–1780, 1997.
- Hofacker, Ivo L. Vienna rna secondary structure server. *Nucleic acids research*, 31(13):3429–3431, 2003.
- Ioffe, Sergey and Szegedy, Christian. Batch normalization: Accelerating deep network training by reducing internal covariate shift. *arXiv preprint arXiv:1502.03167*, 2015.
- Jiang, Peng, Wu, Haonan, Wang, Wenkai, Ma, Wei, Sun, Xiao, and Lu, Zuhong. Mipred: classification of real and pseudo microrna precursors using random forest prediction model with combined features. *Nucleic acids research*, 35(suppl 2):W339–W344, 2007.
- Kang, Wenjing and Friedländer, Marc R. Computational prediction of mirna genes from small rna sequencing data. *Frontiers in bioengineering and biotechnology*, 3, 2015.
- Karpathy, Andrej, Johnson, Justin, and Li, Fei-Fei. Visualizing and understanding recurrent networks. *arXiv preprint arXiv:1506.02078*, 2015.
- Kingma, Diederik P. and Ba, Jimmy. Adam: A method for stochastic optimization. *CoRR*, abs/1412.6980, 2014. URL <http://arxiv.org/abs/1412.6980>.
- Kleptogiannis, Dimitrios, Korfiati, Aigli, Theofilatos, Konstantinos, Likothanassis, Spiros, Tsakalidis, Athanasios, and Mavroudi, Seferina. Where we stand, where we are moving: Surveying computational techniques for identifying mirna genes and uncovering their regulatory role. *Journal of biomedical informatics*, 46(3):563–573, 2013.
- LeCun, Yann, Bengio, Yoshua, and Hinton, Geoffrey. Deep learning. *Nature*, 521(7553):436–444, 2015.
- Lee, Rosalind C, Feinbaum, Rhonda L, and Ambros, Victor. The c. elegans heterochronic gene lin-4 encodes small rnas with antisense complementarity to lin-14. *Cell*, 75(5):843–854, 1993.
- Li, Jiwei, Chen, Xinlei, Hovy, Eduard, and Jurafsky, Dan. Visualizing and understanding neural models in nlp. *arXiv preprint arXiv:1506.01066*, 2015.
- Lorenz, Ronny, Bernhart, Stephan H, Zu Siederdissen, Christian Hoener, Tafer, Hakim, Flamm, Christoph, Stadler, Peter F, and Hofacker, Ivo L. Viennarna package 2.0. *Algorithms for Molecular Biology*, 6(1):1, 2011.

Lyngsø, Rune B. Complexity of pseudoknot prediction in simple models. In *Automata, Languages and Programming*, pp. 919–931. Springer, 2004.

Mathelier, Anthony and Carbone, Alessandra. Mirena: finding micrnas with high accuracy and no learning at genome scale and from deep sequencing data. *Bioinformatics*, 26(18):2226–2234, 2010.

Tempel, Sebastien, Zerath, Benjamin, Zehraoui, Farida,

Tahi, Fariza, et al. mirboost: boosting support vector machines for microrna precursor classification. *RNA*, 21(5):775–785, 2015.

Xue, Chenghai, Li, Fei, He, Tao, Liu, Guo-Ping, Li, Yanda, and Zhang, Xuegong. Classification of real and pseudo microrna precursors using local structure-sequence features and support vector machine. *BMC bioinformatics*, 6(1):310, 2005.